Biochimica et Biophysica Acta 1787 (2009) 113–120

Contents lists available at ScienceDirect

Biochimica et Biophysica Acta

journal homepage: www.elsevier.com/locate/bbabio

Tuning of functional heme reduction potentials in *Shewanella* fumarate reductases

Miguel Pessanha [a], Emma L. Rothery [b], Caroline S. Miles [c], Graeme A. Reid [c], Stephen K. Chapman [b], Ricardo O. Louro [d], David L. Turner [d,e], Carlos A. Salgueiro [a,*], António V. Xavier [d,†]

[a] *Requimte-CQFB, Departamento de Química, Faculdade de Ciências e Tecnologia, Universidade Nova de Lisboa, Campus Caparica, 2829-516 Caparica, Portugal*
[b] *Department of Chemistry, University of Edinburgh, West Mains Road, Edinburgh EH9 3JJ, Scotland, UK*
[c] *Institute of Structural and Molecular Biology, School of Biological Sciences, University of Edinburgh, Mayfield Road, Edinburgh EH9 3JR, Scotland, UK*
[d] *Instituto de Tecnologia Química e Biológica, Universidade Nova de Lisboa, Av. Republica (EAN), 2780-156 Oeiras, Portugal*
[e] *School of Chemistry, University of Southampton, Southampton SO17 1BJ, UK*

ARTICLE INFO

Article history:
Received 19 September 2008
Received in revised form 6 November 2008
Accepted 7 November 2008
Available online 21 November 2008

Keywords:
Respiratory enzyme
Fumarate
Heme
NMR
Redox
Electrostatic interaction

ABSTRACT

The fumarate reductases from *S. frigidimarina* NCIMB400 and *S. oneidensis* MR-1 are soluble and monomeric enzymes located in the periplasm of these bacteria. These proteins display two redox active domains, one containing four *c*-type hemes and another containing FAD at the catalytic site. This arrangement of single-electron redox co-factors leading to multiple-electron active sites is widespread in respiratory enzymes. To investigate the properties that allow a chain of single-electron co-factors to sustain the activity of a multi-electron catalytic site, redox titrations followed by NMR and visible spectroscopies were applied to determine the microscopic thermodynamic parameters of the hemes. The results show that the redox behaviour of these fumarate reductases is similar and dominated by a strong interaction between hemes II and III. This interaction facilitates a sequential transfer of two electrons from the heme domain to FAD via heme IV.

1. Introduction

Shewanella frigidimarina NCIMB400 and *Shewanella oneidensis* MR-1 are gram-negative, facultative anaerobes belonging to the γ subgroup of Proteobacteria, and exhibit a remarkable respiratory flexibility toward a wide range of terminal electron acceptors, including insoluble metal oxides and soluble compounds such as fumarate [1].

Fumarate respiration is accomplished by a highly efficient protein system, including multiredox-center enzymes that participate in this catalytic process. Under anaerobic conditions and using fumarate as the sole terminal electron acceptor *S. oneidensis* and *S. frigidimarina* produce a large quantity of a periplasmic tetraheme flavocytochrome (fcc_3) that acts functionally as a unidirectional terminal fumarate reductase [2]. This enzyme is soluble, monomeric (64 kDa), and its crystal structure reveals that it folds in three domains: the N-terminal heme domain, containing four *c*-types hemes each axially coordinated by two histidines; the flavin domain which contains a non-covalently bound FAD, located close to the active site; and the clamp domain [3,4]. Fumarate reductases catalyse the two-electron, two-proton reduction of fumarate to succinate. The reducing equivalents used for this catalytic process are provided by lactate, formate or H_2, which are metabolic substrates commonly used by *Shewanella* species during anaerobic respiration.

Quinol:fumarate oxidoreductases from other bacteria have been identified as complexes of several subunits, anchored to the inner face of the cytoplasmic membrane. These enzymes contain iron–sulfur centers and FAD [5], as in those reported from *Escherichia coli* [6] and *Wolinella succinogenes* [7,8], and are closely related to succinate: quinone oxidoreductases [9]. However, in contrast, the fumarate reductases from *Shewanella* species reported in this study are unique because they are soluble, monomeric enzymes found in the periplasmic space [10]. This arrangement requires that electrons are supplied from the quinone pool, an activity performed by a membrane bound *c*-type cytochrome called CymA, which has an N-terminal α-helical membrane anchor associated with the inner membrane, and a globular tetraheme periplasmic domain [11,12]. It was shown by Schwalb et al. [12] that CymA efficiently reduces the fumarate reductase and it is most likely that fcc_3 accepts electrons from CymA by using the exposed hemes.

Interestingly, despite the differences in cell location and architecture, the structures from several fumarate reductases, namely from *Shewanella* species [3,4,13], *E. coli* [6] and *W. succinogenes* [7], reveal that the enzyme active site presents a common architecture and the important catalytic residues close to the FAD active site are conserved.

Abbreviations: fcc_3, flavocytochrome c_3; $Sffcc_3$, flavocytochrome c_3 from *S. frigidimarina*; $Sofcc_3$, flavocytochrome c_3 from *S. oneidensis*

* Corresponding author. Departamento Química, Faculdade de Ciências e Tecnologia, Universidade Nova de Lisboa, Campus Caparica, 2829-516 Caparica, Portugal. Tel.: +351 212 948 300; fax: +351 212 948 385.
E-mail address: csalgueiro@dq.fct.unl.pt (C.A. Salgueiro).

† Deceased 7th May 2006.

0005-2728/$ – see front matter © 2008 Elsevier B.V. All rights reserved.
doi:10.1016/j.bbabio.2008.11.007

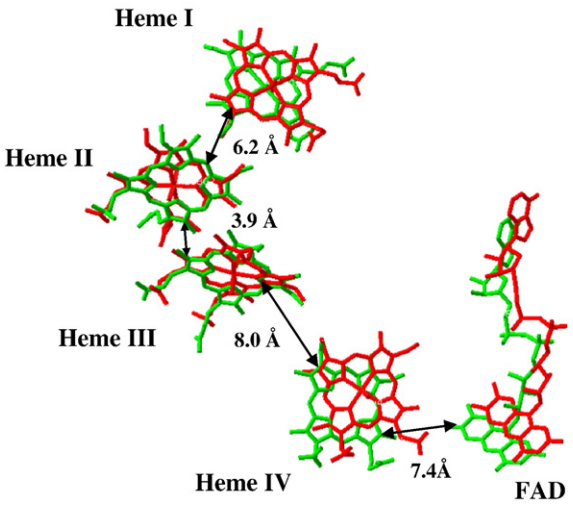

Fig. 1. Structural features of fcc_3 from *S. frigidimarina* and *S. oneidensis* redox centers [3,4]. The spatial disposition of the five redox centers of $Sffcc_3$ and $Sofcc_3$ are shown in green and red, respectively. To avoid overcrowding the figure, only the edge-to-edge distances between neighboring centers for $Sffcc_3$ are shown.

As a consequence, a common mechanism for fumarate reduction in this family of enzymes has been proposed [4,14–18].

In *Shewanella* spp. fumarate reductases the redox centers are very close (<8 Å) and in a quasi-linear spatial arrangement, (see Fig. 1), therefore electron transfer within the tetraheme domain is fast. Electron flow from the heme domain to the FAD must proceed via heme IV, which controls the passage of electrons from the heme domain to the flavin [19]. An array of single electron redox centers leading to a multi-electron active site is found in several respiratory enzymes such as the oxygen oxidoreductases [20], the hydrogenases [21] or the CO dehydrogenases [22].

Although the fumarate reductase from *S. frigidimarina* has been investigated with respect to its biochemical, thermodynamic, kinetic, and mechanistic features [14,16–19,23–28], the microscopic thermodynamic characterization of the individual hemes, including their pairwise interactions, has not been reported. To date, measurements with this level of detail have been restricted to proteins of modest size, typically less than 16 kDa [29–41]. This work is the first example of using NMR techniques for the microscopic thermodynamic analysis of redox proteins of moderate size, opening the way to the detailed characterization of a much wider range of redox proteins. The results presented here for the fumarate reductases from *S. oneidensis* and *S. frigidimarina* allow the proposal of a common functional mechanism for the transfer of two electrons to the FAD active site by a chain of single electron centers.

2. Materials and methods

2.1. Bacterial growth and protein purification

S. oneidensis MR-1 and *S. frigidimarina* NCIMB400 cells were grown and the tetraheme flavocytochromes c_3 were purified as previously described in [11] and [23], respectively.

2.2. NMR sample preparation

The protein solutions were exchanged several times into 99.9% ^2H_2O using ultrafiltration methods (Amicon; YM-10) thus removing all trace of FAD. Samples with a final protein concentration of 0.5 mM were used. The ionic strength was adjusted to 100 mM by addition of a NaCl solution in ^2H_2O. Reduced samples were obtained by the reaction of the

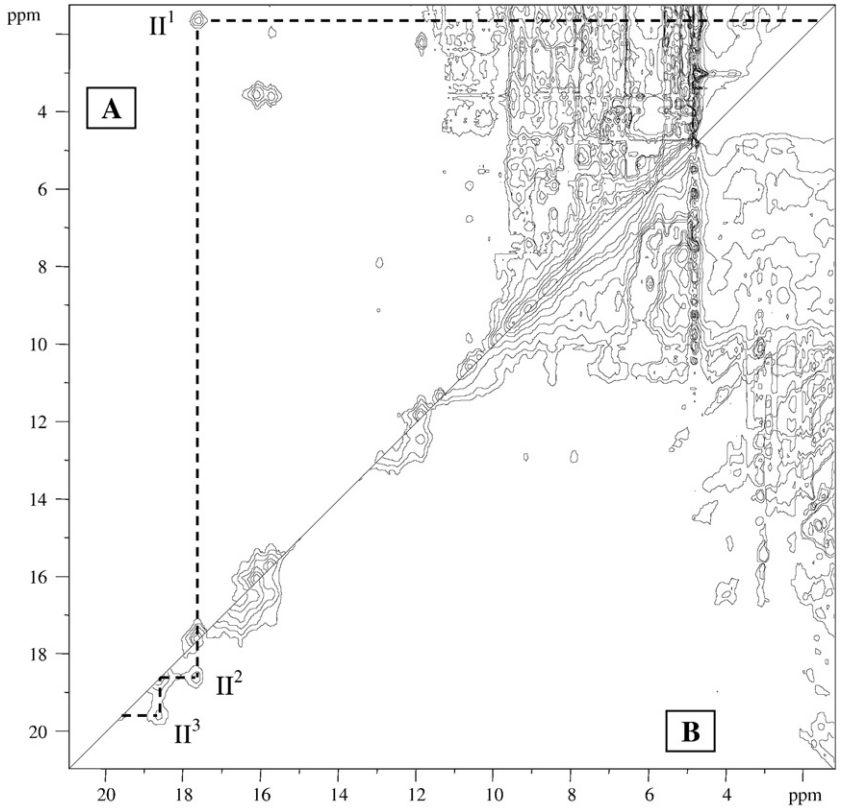

Fig. 2. Region of 2D-EXSY NMR spectra of $Sofcc_3$ at different oxidation levels at 298 K and pH 7.2. (A) The spectrum shows cross peaks connecting oxidation stages 0–1. (B) the spectrum shows cross peaks connecting oxidation stages 1–3. The lines connect signals for one methyl group of heme II (dashed lines) in different oxidation stages. The Roman and Arabic numbers indicate the heme group and the oxidation stages, respectively.

oxidized protein with gaseous hydrogen in the presence of catalytic amounts of the enzyme hydrogenase (Fe and NiFe isolated from *Desulfovibrio vulgaris* and *Desulfovibrio gigas*, respectively). Partially oxidized samples were obtained by flushing the excess hydrogen from reduced samples with argon and then adding controlled amounts of air into the NMR tube with a syringe through the rubber cap as previously described [35]. In the reduced and intermediate stages of oxidation the pH was adjusted inside an anaerobic glove box (Mbraun MB 150 I) with argon atmosphere circulation to avoid the reoxidation of the sample. The pH values reported are direct meter readings without correction for the isotope effect [42].

2.3. NMR spectroscopy

^{1}H-NMR spectra were obtained in a 500 MHz Bruker DRX500 spectrometer equipped with a 5 mm inverse detection probe head with internal B_0 gradient coils. All the NMR experiments were carried out at 298 K. Chemical shifts are reported in parts per million (ppm), and spectra were calibrated using the water signal as an internal reference. All values are reported relative to TMS. The program XEASY [43] was used to display the 2D-NMR spectra and assign signals.

2.3.1. NMR of oxidized fcc3 from S. oneidensis

One-dimensional (1D) NMR spectra of *fcc*$_3$ from *S. oneidensis* were acquired at pH 7.2 with 128 scans and 64 k data points to cover a sweep width of 32 kHz.

2.3.2. NMR redox titrations of fcc3 from S. frigidimarina and S. oneidensis

In order to establish the complete pattern of oxidation for each heme, 2D-EXSY NMR data sets were collected in the intermediate states of oxidation in the pH range 7.0–8.5. These spectra were acquired with a 25 ms mixing time using and 4096 (t_2)×1024 (t_1) data points spanning a sweep width of 32 kHz, with 128 scans per increment. A selective pulse of at least 600 ms was used for water presaturation in all experiments.

2.4. Predictions of chemical shifts for the heme methyls

^{1}H paramagnetic chemical shifts of the heme methyls for *fcc*$_3$ from *S. oneidensis* were calculated from the empirical equation reported in the literature [44] using the geometry of the heme axial ligands in the crystal structure [3]. ^{1}H diamagnetic chemical shifts of the heme methyls for *fcc*$_3$ from *S. oneidensis* were calculated by correcting the heme methyl reference shift (3.48 ppm which is an average of values available for different cytochromes [45]) with the ring current shifts calculated from the crystal structure [3] using a modified version of the software TOTAL [46].

2.5. Redox titrations followed by visible spectroscopy

For both enzymes, anaerobic redox titrations followed by visible spectroscopy were performed as described previously [32]. Protein solutions of ca. 16 μM in 100 mM TRIS/maleate buffer at pH 7.0 and 8.5 were used. For each pH value the redox titrations were performed in both oxidative and reductive directions to check for hysteresis. In order to ensure a good equilibrium between the redox centers and the working electrode [47], a mixture of the following redox mediators was added to the protein solution, all at ca. 2 μM final concentration: anthraquinone-2-7-disulfonate, 2-hydroxy-1-4 naphthoquinone, anthraquinone-2-sulfonate, safranine O, diquat, benzylviologen, neutral red, methylviologen, methylene blue, gallocyanine, indigo tetrasulfonate, indigo trisulfonate and indigo disulfonate. Solution potentials were measured using a combined Pt/Ag/AgCl electrode. Visible spectra were recorded at 298 K in a Shimadzu UV-1203 spectrophotometer, placed inside an anaerobic glove box (Mbraun MB 150 I) under an argon atmosphere, in order to keep the O_2 level below 0.5 ppm. The reduced fraction of the *fcc*$_3$ was obtained using the α band peak located at 552 nm. The optical contribution of the mediators was subtracted by measuring the height of the α peak relative to the straight line connecting the two isosbestic points flanking the α band, as previously described [32,48].

2.6. Thermodynamic modelling

The thermodynamic model used to determine the thermodynamic parameters of both fumarate reductases was described previously [31].

3. Results

The crystal structures of the tetraheme flavocytochromes from *S. oneidensis* [3] and *S. frigidimarina* [4] show that all heme irons have

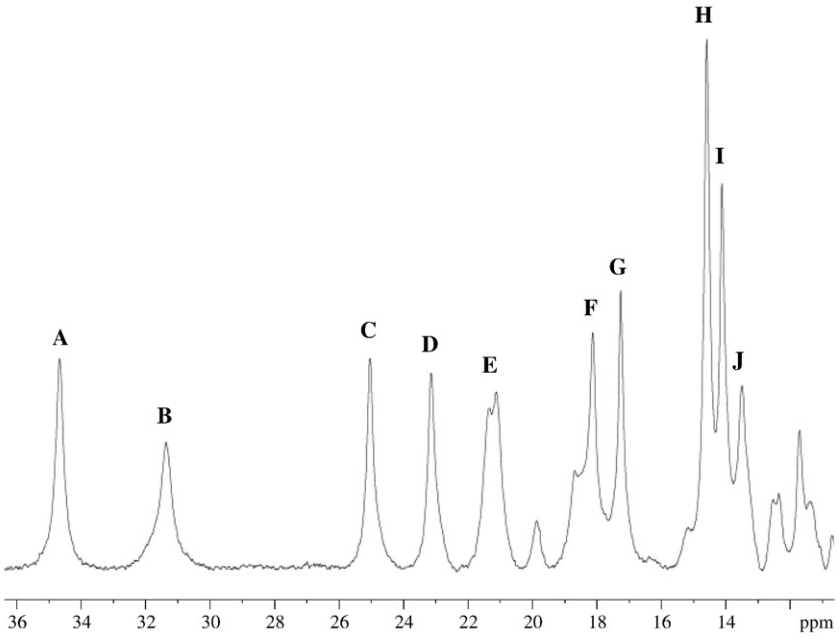

Fig. 3. Low-field region of 500 MHz 1D-^{1}H NMR spectra of the oxidized *Sofcc*$_3$ at pH 7.2 and 298 K. The heme methyl signals are labelled alphabetically (A–J).

Table 1
Redox-dependent ^{1}H heme methyl chemical shifts (A) and heme oxidation fraction (B) of *S. oneidensis* flavocytochrome c_3, at pH 8.5 and 298 K

A

Oxidation stage	Chemical shift (ppm)									
	A	B	C	D	E	F	G	H	I	J
0	(3.48)	(3.48)	(3.48)	(3.48)	1.66	3.55	(3.48)	(3.48)	(3.48)	2.24
1	n.o.	n.o.	n.o.	n.o.	17.63	16.14	n.o.	n.o.	n.o.	11.86
2	8.38	15.44	n.o.	n.o.	18.52	16.52	10.38	n.o.	n.o.	12.50
3	20.05	22.89	16.93	16.45	19.80	17.10	16.83	9.37	9.38	12.91
4	34.68	31.51	25.04	23.26	21.30	18.14	17.40	14.72	14.23	13.57

B

Oxidation stage	x_i									
	Heme I			Heme II			Heme III			Heme IV
	A	H	I	E	F	J	B	C	D	G
0	0	0	0	0	0	0	0	0	0	0
1	n.a.	n.a.	n.a.	0.81	0.86	0.85	n.a.	n.a.	n.a.	n.a.
2	0.16	n.a.	n.a.	0.86	0.89	0.91	0.43	n.a.	n.a.	0.50
3	0.53	0.52	0.55	0.92	0.93	0.94	0.69	0.62	0.66	0.96
4	1	1	1	1	1	1	1	1	1	1

The heme methyls A–J are labelled according to their position in the oxidized form. The heme fractions of oxidation, x_i, in each stage of oxidation are calculated according to the equation $x_i=(\delta_i-\delta_0)/(\delta_4-\delta_0)$, where δ_i, δ_0, and δ_4 are the observed chemical shift of the heme methyl in stage *i*, *0*, and *4*, respectively [54]. The chemical shifts indicated in parenthesis are assumed values for the diamagnetic reference for heme methyl protons [45].
n.o. — not observed; n.a. — not applicable.

bis-histidinyl axial coordination in both enzymes. Thus, they are diamagnetic (Fe(II), S=0) in the reduced state and paramagnetic (Fe (III), S=1/2) in the oxidized state. For proteins of moderate size, these properties ensure that well-resolved NMR spectra are obtained in both oxidation states, thus facilitating the assignment of heme signals and the determination of their relative order of oxidation. However, as previously reported for the *fcc*$_3$ from *S. frigidimarina* [49], due to the enzyme molecular weight (c.a. 64 kDa) and the associated slow tumbling rate, which broadens the signals, it was not possible to obtain sufficiently well-resolved spectra to assign the heme resonances unequivocally. Even so, it was possible to observe cross-peaks connecting heme signals in partially oxidized samples using 2D-EXSY NMR experiments for *fcc*$_3$ from *S. frigidimarina* (*Sffcc*$_3$) and *S. oneidensis* (*Sofcc*$_3$) (Fig. 2). Minimizing the line widths involved adjusting the protein concentration, the ionic strength of the sample and the temperature to maximize the tumbling rate while keeping the intermolecular electron exchange rates slow on the NMR time scale. For some hemes it was not possible to observe all of the exchange signals in the experimental pH range (7.0–8.5), which may have been caused by additional broadening due to the exchange process between the protonated and deprotonated forms at a solution pH close to the *pKa* of redox-linked acid–base centers [31]. However, the thermodynamic parameters can be accurately determined (see below) since the degree of oxidation of three of the hemes at each oxidation stage, together with the overall oxidation of the protein, determines the degree of oxidation of the fourth heme.

Under these optimized experimental conditions both proteins exhibit fast intramolecular ($>10^5$ s^{-1}) and slow intermolecular ($<10^3$ s^{-1}) electron exchange rates on the NMR time scale. In these conditions, signals from the sixteen redox microstates are averaged in five macroscopic oxidation stages, each comprising the group of microstates with the same number (0–4) of oxidized hemes [29]. The paramagnetic chemical shift of each heme substituent in each oxidation stage is proportional to the level of oxidation of that specific heme in that stage and, consequently, only one signal for each heme needs to be followed to monitor the degree of oxidation of the hemes during a redox titration [29].

From the analysis of 2D-EXSY NMR spectra of partially oxidized samples it was possible to follow several heme methyl resonances in the different oxidation stages to their final positions in the oxidized protein and, thus, to monitor the heme redox behaviour of both enzymes. The strategy used to assign the heme methyl resonances for *Sffcc*$_3$ was previously reported [49]. In the case of *Sofcc*$_3$, ten heme methyl resonances labelled (A–J) were followed (Fig. 3 and Table 1). The different patterns of oxidation showed by these signals were grouped into four categories and cross-assigned to the structure (see below). As mentioned previously it was not possible to assign all the heme substituents specifically in either the fully reduced or fully oxidized states. However, assignment of the signals to specific hemes was possible using a strategy that relies on the crystal structures to predict the chemical shift of the heme methyl signals in oxidized and reduced states.

3.1. Cross-assignment of *Sofcc*$_3$ heme signals to specific hemes in the structure

The first step in the assignment strategy was based on the calculation of the ^{1}H paramagnetic chemical shifts of each heme methyl group (Table 2). Table 2 shows that the most shifted signal is predicted to be heme methyl 18^{1}CH$^{\mathrm{I}}_3$ (33.4 ppm), but the experimental data (Table 1) show that two signals, A and B, are located in this region (34.7 ppm and 31.5 ppm, respectively). However, the heme methyl reoxidation patterns (Table 1) show that the patterns of signals A and B are different, indicating that these signals belong to different hemes. The reoxidation pattern of signal B is similar to those of methyl signals C and D, which have chemical shifts of 25.0 ppm and 23.3 ppm, respectively. Only heme III is predicted to have three heme methyl signals above 24.0 ppm (Table 2), which correlates well with signals B, C and D. Consequently, signal A was assigned with confidence to 18^{1}CH$^{\mathrm{I}}_3$ and methyls B, C and D to heme III.

Table 2
Predicted ^{1}H chemical shifts for each heme methyl of *fcc*$_3$ from *S. oneidensis* in the reduced (diamagnetic) and oxidized (paramagnetic) states

Heme methyl	Reduced				Oxidized			
	Heme				Heme			
	I	II	III	IV	I	II	III	IV
2^{1}CH$_3$	3.57	2.37	2.77	3.48	12.10	20.40	24.00	19.90
7^{1}CH$_3$	3.00	3.59	3.68	3.44	15.50	6.60	7.10	7.00
12^{1}CH$_3$	3.35	3.58	3.56	3.57	13.50	21.80	25.40	21.30
18^{1}CH$_3$	3.46	1.97	2.01	3.45	33.40	12.50	24.10	12.10

The heme methyls are numbered according to IUPAC-IUB nomenclature for tetrapyrroles [55].

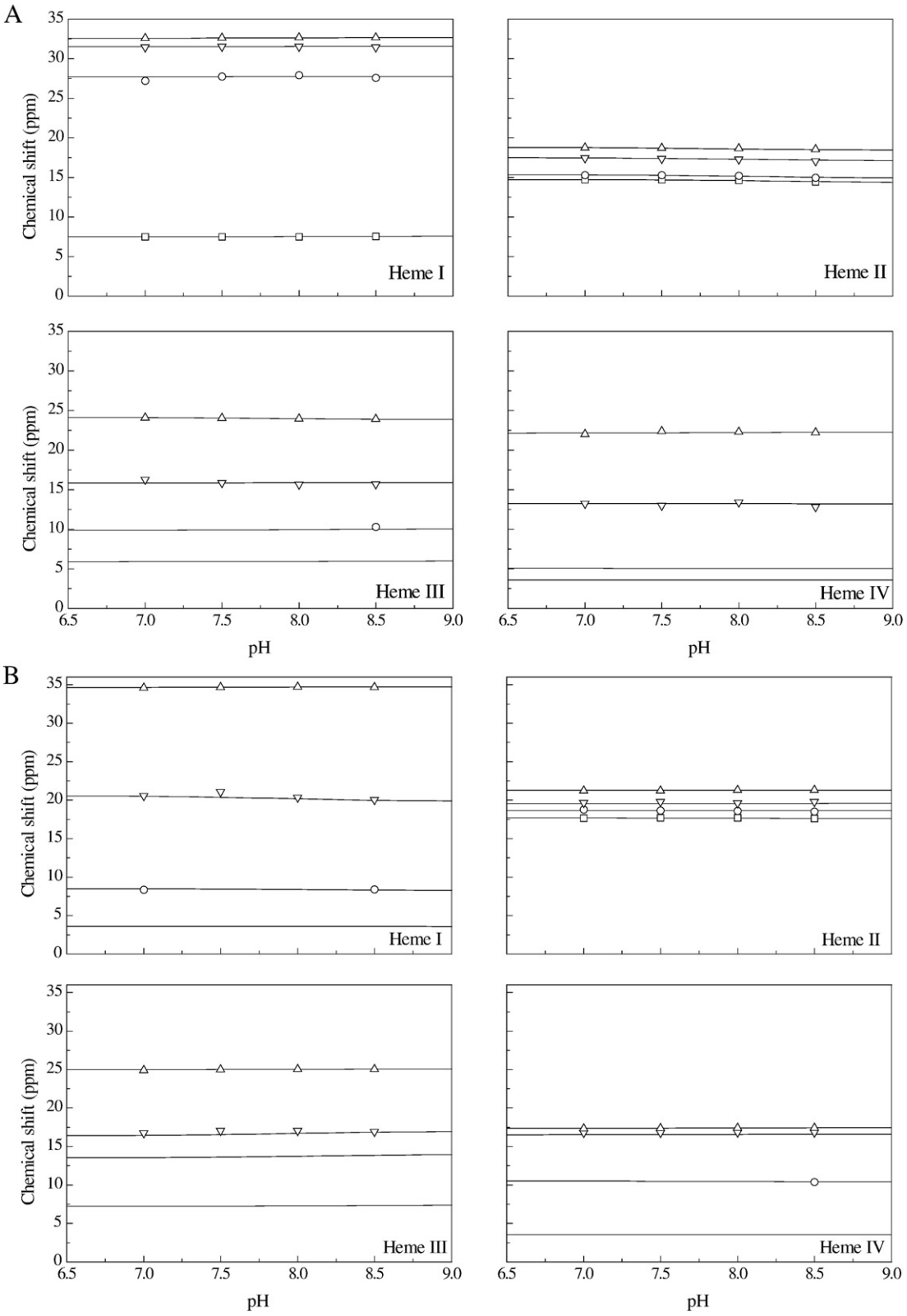

Fig. 4. The pH dependence of the chemical shift of heme methyl group resonances CH_3^I, CH_3^{II}, CH_3^{III} and CH_3^{IV} of *Sffcc*$_3$ (A) and *Sofcc*$_3$ (B). Squares correspond to stage 1 of oxidation, circles to stage 2, downward-pointing triangles to stage 3, and upward-pointing triangles to stage 4. The solid lines show the result of simultaneous fitting of the NMR and visible data.

The remaining heme methyl signals (E–J) include signals from hemes II and IV, but these hemes cannot be discriminated on the basis of the predicted ^{1}H chemical shifts of the oxidized protein (Table 2). Nonetheless, the ^{1}H diamagnetic chemical shifts predicted for each heme methyl group (Table 2) are quite distinct for hemes II and IV. For heme II, two methyls (18^1CH_3 and 2^1CH_3) are predicted at 1.97 and 2.37 ppm, respectively, whereas predictions for all heme methyls from heme IV are close to the reference value of 3.48 ppm. In 2D-EXSY NMR

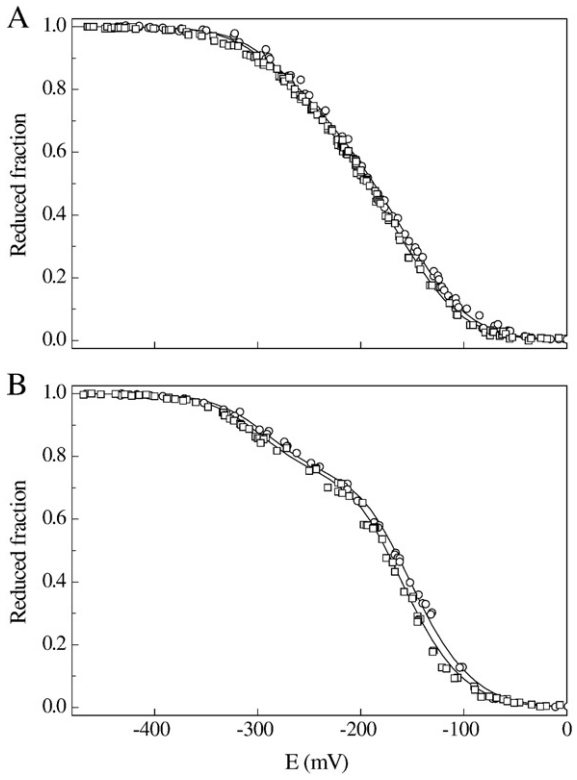

Fig. 5. Reduced fraction of *Sffcc*$_3$ (A) and *Sofcc*$_3$ (B) determined by visible spectroscopy at pH 7.0 (circles) and 8.5 (squares). The solid lines were determined from the simultaneous fitting of the NMR and visible data.

spectra of partially oxidized samples two heme methyl signals, E and J show cross-peaks to stage 0 at 1.66 and 2.24 ppm, respectively (Table 1). The pattern of reoxidation of these signals is similar (Table 1), as expected for methyls from the same heme, and their diamagnetic chemical shifts are in agreement with the predicted values for heme II. Therefore, signals E and J were assigned to heme II. Since the oxidation pattern corresponding to the heme signal G was different from those observed for all the other heme signals (Table 1), it was assigned to heme IV. Finally, signal F was also assigned to heme II and signals H and I to heme I since they show similar oxidation patterns to those of signals E and J, and to signal A, respectively.

This assignment strategy allowed four different oxidation patterns to be unambiguously assigned to heme groups in the crystal structure of *Sofcc*$_3$. Assignment of the signals of *Sffcc*$_3$ was previously reported [49].

3.2. Thermodynamic characterization of *Soffcc*$_3$ and *Sofcc*$_3$

As mentioned above, and as shown in previous works [29,31], the variation of the paramagnetic chemical shifts of only one substituent per heme is needed to map the oxidation patterns of that particular heme. For *Soffcc*$_3$ *and Sofcc*$_3$, at least one methyl group from each heme is well shifted from the main envelope of resonances in the oxidized form and thus not subject to signal overlap. The pH dependence of the paramagnetic chemical shifts each heme methyl group and the data obtained for redox titrations followed by visible spectroscopy were fitted to the thermodynamic model described previously [31] to determine the properties of both tetraheme flavocytochromes. The fittings of both NMR and visible data are shown in Figs. 4 and 5. The experimental uncertainty of the NMR data was estimated from the line width of each signal, and the visible data points were given an uncertainty of 3% of the total change in absorbance.

The thermodynamic parameters for *Sffcc*$_3$ *and Sofcc*$_3$ are listed in Table 3, and the titration curves of the individual hemes determined from the experimental parameters are shown in Fig. 6.

4. Discussion

The analysis of the thermodynamic parameters obtained for both flavocytochromes (Table 3) shows that the microscopic reduction potentials of the hemes are negative and cover a similar range: −148 to −270 mV and −145 to −286 mV for *Sffcc*$_3$ and *Sofcc*$_3$, respectively. The individual reduction potentials are similar with exception of that of heme I which is more positive in *Sofcc*$_3$ and account for the different shape of the redox titration curves of the two proteins (Fig. 5). In both proteins, heme II has most negative reduction potential and is therefore the heme to become more oxidized in the first oxidation step. The effect of protonation on the heme reduction potentials (redox–Bohr interactions) is small and of similar magnitude for all heme groups in both flavocytochromes (see Table 3 and Fig. 4).

For both proteins, the heme redox interactions (Table 3) are dominated by the interaction between hemes II and III (+65 and +95 mV, for *Sffcc*$_3$ and *Sofcc*$_3$, respectively). Fig. 6 shows that the individual titration curves do not display the shape of a Nernst curve and in some cases cross over are observed, an indication that the affinity for electrons of each heme is influenced by the redox state of neighboring hemes. The clearest example of such modulation is observed in the oxidative curve of heme III which shifts towards higher reduction potentials as the oxidation of heme II progresses, due to their very strong negative homo-cooperativity (Fig. 6). Consequently, in the first oxidation stage (loss of the first electron by the tetraheme domain) the reduction potential of heme III is increased so that it remains essentially reduced (*cf.* the oxidation fraction at 25% for the global protein with those of hemes II and III in Fig. 6).

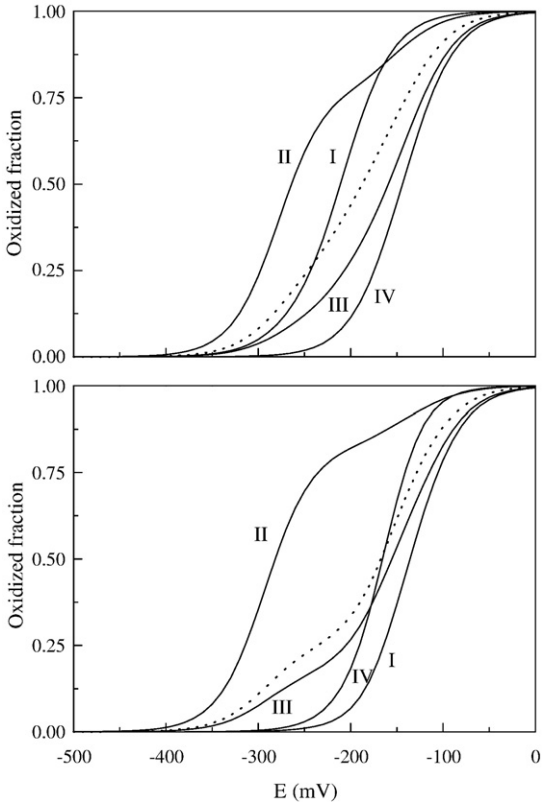

Fig. 6. Oxidized fractions of the individual hemes of *Sffcc*$_3$ (A) and *Sofcc*$_3$ (B) at pH 7.2. The curves were calculated as a function of the solution reduction potential using the parameters listed in Table 3. The dashed lines represent the global oxidation fraction.

Table 3
Thermodynamic parameters determined for *Sffcc$_3$* (A) *and Sofcc$_3$* (B)

A

	Energies (meV)				
	Heme I	Heme II	Heme III	Heme IV	Ionisable center
Heme I	**−228 (5)**	23 (3)	3 (3)	−2 (6)	−10 (4)
Heme II		**−270 (5)**	65 (2)	0 (3)	−10 (4)
Heme III			**−223 (6)**	12 (2)	−11 (4)
Heme IV				**−148 (8)**	−10 (4)
Ionisable center					**504 (36)**

B

	Energies (meV)				
	Heme I	Heme II	Heme III	Heme IV	Ionisable center
Heme I	**−145 (8)**	17 (4)	22 (4)	−23 (4)	−11 (5)
Heme II		**−286 (8)**	95 (5)	3 (5)	−13 (5)
Heme III			**−247 (9)**	−3 (3)	−14 (5)
Heme IV				**−160 (9)**	−12 (6)
Ionisable center					**505 (54)**

Diagonal terms (in bold) represent the oxidation energies of the four hemes and the deprotonating energies for the ionisable center in the fully reduced and protonated protein. The conversion factor from an energy in meV to pH units is $0.001 \times F/(2.3RT)$, which yields approximately $pK_{red} \approx 8.5$ in both proteins. The off-diagonal elements represent the redox and redox–Bohr interaction energies between the five centers. Standard errors are given in parenthesis.

The close similarity between Fig. 5A and Fig. 3 of Turner et al. [2] shows that the presence of FAD does not alter the redox properties of the hemes significantly. Indeed, the scale of the interactions measured here together with the structural data summarized in Fig. 1 predicts an anti-cooperative interaction of ca. 10 mV between FAD and heme IV and little or no effect on the other hemes. Comparison with the voltammetric results of Turner et al. [2] is also complicated by the interaction of the redox centers with the electrode surface. However, the FAD is less exposed than the hemes and we may assume that the measured reduction potential, ca. −100 mV at pH 6.0 and −200 mV at pH 8.0, is similar to its value in solution [2]. The redox potential of the FAD is therefore close to those of hemes III and IV, thus ensuring rapid electron transfer.

These observations can be rationalized in functional terms, knowing that the semiquinone state of the FAD is not observed in these fumarate reductases [2]. Oxidation of FAD leads to a sequential two-electron transfer from the heme domain to FAD, via heme IV, when both hemes III and IV are thermodynamically biased to be reduced. As the first electron is taken from heme IV by FAD, heme IV can readily be re-reduced by the neighboring heme III, thus facilitating the transfer of the second electron for reduction of FAD. The fast kinetics of electron transfer in this arrangement ($>10^5$ s^{-1} for both *Sffcc$_3$* and *Sofcc$_3$*) ensures that the lifetime of a semiquinone, and the possible consequence of producing reactive oxygen species, is minimized. This interpretation of the data collected for both *Shewanella* fumarate reductases, and a previous mechanistic proposal [49], are in good agreement with observations made for the membrane bound fumarate reductase from *E. coli*, where the authors propose that having the proximal ([2Fe–2S]) and the medial ([4Fe–4S]) clusters loaded with electrons ensures that the system is poised for the supply of two electrons to the FAD for catalysis [50].

As previously demonstrated by Schwalb et al. [12], re-reduction of the *fcc$_3$* tetraheme domain is mediated by CymA, and heme I of *fcc$_3$* is a likely candidate for electron uptake, though all four hemes have some solvent exposure. There is no simple explanation for the difference in mid-point potentials of heme I in *fcc$_3$*, though it could be related with optimization of electron uptake from the respective forms of CymA since all other hemes show similar redox properties. These include the strong redox interaction between hemes II and III, which is responsible for maintaining a high electron affinity of hemes III and IV in the catalytically relevant redox stages, enhancing the directionality of the intramolecular electron transfer from the heme domain to FAD. The similarity in the properties of *Sffcc$_3$* and *Sofcc$_3$* is even more striking given the differences between these and small tetraheme proteins that have structures similar to the heme domain of *fcc$_3$*, and the differences between those proteins [51,52].

In conclusion, this work describes the detailed microscopic thermodynamic characterization of the redox centers, as well their interactions, for two multiredox center proteins larger than 64 kDa. This represents a considerable expansion in the range of sizes of redox proteins that have been studied in detail using NMR spectroscopy. It has been shown by Dutton et al. [53] that the distance between the redox centers (below 14 Å) is the most important factor that provides robustness to electron transfer in multi-redox center enzymes. This work addresses the additional requirement of redox potentials that are properly tuned. The data reveal how the thermodynamic properties of the individual hemes, modulated by the oxidation and reduction of their closely spaced neighbors, can favor delivery of electrons to a two-electron active site by an array of single electron cofactors.

Acknowledgments

This work was supported by research grants PPCDT/BIA-PRO/58722/2004, POCI/QUI/58985/2004, POCI/QUI/60060/2004, and PPCDT/QUI/60060/2004 from Fundação para a Ciência e a Tecnologia (Portugal). Miguel Pessanha acknowledges FCT, Portugal, for a doctoral fellowship (SFRH/5229/2001). Prof. Teresa Catarino is acknowledged for very fruitful discussions.

References

[1] K.H. Nealson, A. Belz, B. McKee, Breathing metals as a way of life: geobiology in action, Antonie Van Leeuwenhoek 81 (2002) 215–222.
[2] K.L. Turner, M.K. Doherty, H.A. Heering, F.A. Armstrong, G.A. Reid, S.K. Chapman, Redox properties of flavocytochrome c_3 from *Shewanella frigidimarina* NCIMB400, Biochemistry 38 (1999) 3302–3309.
[3] D. Leys, A.S. Tsapin, K.H. Nealson, T.E. Meyer, M.A. Cusanovich, J.J. Van Beeumen, Structure and mechanism of the flavocytochrome *c* fumarate reductase of *Shewanella putrefaciens* MR-1, Nat. Struct. Biol. 6 (1999) 1113–1117.
[4] P. Taylor, S.L. Pealing, G.A. Reid, S.K. Chapman, M.D. Walkinshaw, Structural and mechanistic mapping of a unique fumarate reductase, Nat. Struct Biol. 6 (1999) 1108–1112.
[5] R.S. Lemos, A.S. Fernandes, M.M. Pereira, C.M. Gomes, M. Teixeira, Quinol: fumarate oxidoreductases and succinate:quinone oxidoreductases: phylogenetic relationships, metal centres and membrane attachment, Biochim. Biophys. Acta 1553 (2002) 158–170.
[6] T.M. Iverson, C. Luna-Chavez, G. Cecchini, D.C. Rees, Structure of the *Escherichia coli* fumarate reductase respiratory complex, Science 284 (1999) 1961–1966.
[7] C.R. Lancaster, A. Kroger, M. Auer, H. Michel, Structure of fumarate reductase from *Wolinella succinogenes* at 2.2 Å resolution, Nature 402 (1999) 377–385.
[8] C. Kortner, F. Lauterbach, D. Tripier, G. Unden, A. Kroger, *Wolinella succinogenes* fumarate reductase contains a dihaem cytochrome *b*, Mol. Microbiol. 4 (1990) 855–860.
[9] T. Ohnishi, C.C. Moser, C.C. Page, P.L. Dutton, T. Yano, Simple redox-linked proton-transfer design: new insights from structures of quinol-fumarate reductase, Structure 8 (2000) R23–32.
[10] C.J. Morris, A.C. Black, S.L. Pealing, F.D. Manson, S.K. Chapman, G.A. Reid, D.M. Gibson, F.B. Ward, Purification and properties of a novel cytochrome: flavocytochrome *c* from *Shewanella putrefaciens*, Biochem. J. 302 (1994) 587–593.
[11] C. Schwalb, S.K. Chapman, G.A. Reid, The membrane-bound tetrahaem c-type cytochrome CymA interacts directly with the soluble fumarate reductase in *Shewanella*, Biochem. Soc. Trans. 30 (2002) 658–662.
[12] C. Schwalb, S.K. Chapman, G.A. Reid, The tetraheme cytochrome CymA is required for anaerobic respiration with dimethyl sulfoxide and nitrite in *Shewanella oneidensis*, Biochemistry 42 (2003) 9491–9497.
[13] V. Bamford, P.S. Dobbin, D.J. Richardson, A.M. Hemmings, Open conformation of a flavocytochrome c_3 fumarate reductase, Nat. Struct. Biol, 6 (1999) 1104–1107.
[14] M.K. Doherty, S.L. Pealing, C.S. Miles, R. Moysey, P. Taylor, M.D. Walkinshaw, G.A. Reid, S.K. Chapman, Identification of the active site acid/base catalyst in a bacterial fumarate reductase: a kinetic and crystallographic study, Biochemistry 39 (2000) 10695–10701.
[15] G.A. Reid, C.S. Miles, R.K. Moysey, K.L. Pankhurst, S.K. Chapman, Catalysis in fumarate reductase, Biochim. Biophys. Acta 1459 (2000) 310–315.
[16] C.G. Mowat, R. Moysey, C.S. Miles, D. Leys, M.K. Doherty, P. Taylor, M.D. Walkinshaw, G.A. Reid, S.K. Chapman, Kinetic and crystallographic analysis of the key active site acid/base arginine in a soluble fumarate reductase, Biochemistry 40 (2001) 12292–12298.

[17] K.L. Pankhurst, C.G. Mowat, C.S. Miles, D. Leys, M.D. Walkinshaw, G.A. Reid, S.K. Chapman, Role of His505 in the soluble fumarate reductase from *Shewanella frigidimarina*, Biochemistry 41 (2002) 8551–8556.
[18] C.G. Mowat, K.L. Pankhurst, C.S. Miles, D. Leys, M.D. Walkinshaw, G.A. Reid, S.K. Chapman, Engineering water to act as an active site acid catalyst in a soluble fumarate reductase, Biochemistry 41 (2002) 11990–11996.
[19] E.L. Rothery, C.G. Mowat, C.S. Miles, M.D. Walkinshaw, G.A. Reid, S.K. Chapman, Histidine 61: an important heme ligand in the soluble fumarate reductase from *Shewanella frigidimarina*, Biochemistry 42 (2003) 13160–13169.
[20] A.F. Verissimo, F.L. Sousa, A.M. Baptista, M. Teixeira, M.M. Pereira, Thermodynamic redox behavior of the heme centers of cbb_3 heme-copper oxygen reductase from *Bradyrhizobium japonicum*, Biochemistry 46 (2007) 13245–13253.
[21] J.C. Fontecilla-Camps, A. Volbeda, C. Cavazza, Y. Nicolet, Structure/function relationships of [NiFe]- and [FeFe]-hydrogenases, Chem. Rev. 107 (2007) 4273–4303.
[22] T.I. Doukov, T.M. Iverson, J. Seravalli, S.W. Ragsdale, C.L. Drennan, A Ni–Fe–Cu center in a bifunctional carbon monoxide dehydrogenase/acetyl-CoA synthase, Science 298 (2002) 567–572.
[23] S.L. Pealing, M.R. Cheesman, G.A. Reid, A.J. Thomson, F.B. Ward, S.K. Chapman, Spectroscopic and kinetic studies of the tetraheme flavocytochrome *c* from *Shewanella putrefaciens* NCIMB400, Biochemistry 34 (1995) 6153–6158.
[24] S.L. Pealing, A.C. Black, F.D. Manson, F.B. Ward, S.K. Chapman, G.A. Reid, Sequence of the gene encoding flavocytochrome *c* from *Shewanella putrefaciens*: a tetraheme flavoenzyme that is a soluble fumarate reductase related to the membrane-bound enzymes from other bacteria, Biochemistry 31 (1992) 12132–12140.
[25] G.A. Reid, E.H. Gordon, A.E. Hill, M. Doherty, K. Turner, R. Holt, S.K. Chapman, Structure and function of flavocytochrome c_3, the soluble fumarate reductase from *Shewanella* NCIMB400, Biochem. Soc. Trans. 26 (1998) 418–421.
[26] A.K. Jones, R. Camba, G.A. Reid, S.K. Chapman, F.A. Armstrong, Interruption and time-resolution of catalysis by a flavoenzyme using fast scan protein film voltammetry, J. Am. Chem. Soc. 122 (2000) 6494–6495.
[27] L.J. Jeuken, A.K. Jones, S.K. Chapman, G. Cecchini, F.A. Armstrong, Electron-transfer mechanisms through biological redox chains in multicenter enzymes, J. Am. Chem. Soc. 124 (2002) 5702–5713.
[28] E.L. Rothery, C.G. Mowat, C.S. Miles, S. Mott, M.D. Walkinshaw, G.A. Reid, S.K. Chapman, Probing domain mobility in a flavocytochrome, Biochemistry 43 (2004) 4983–4989.
[29] H. Santos, J.J. Moura, I. Moura, J. LeGall, A.V. Xavier, NMR studies of electron transfer mechanisms in a protein with interacting redox centres: *Desulfovibrio gigas* cytochrome c_3, Eur. J. Biochem. 141 (1984) 283–296.
[30] R.O. Louro, I. Pacheco, D.L. Turner, J. LeGall, A.V. Xavier, Structural and functional characterization of cytochrome c_3 from *D. desulfuricans* ATCC 27774 by ^{1}H-NMR, FEBS Lett. 390 (1996) 59–62.
[31] D.L. Turner, C.A. Salgueiro, T. Catarino, J. Legall, A.V. Xavier, NMR studies of cooperativity in the tetrahaem cytochrome c_3 from *Desulfovibrio vulgaris*, Eur. J. Biochem. 241 (1996) 723–731.
[32] R.O. Louro, T. Catarino, J. LeGall, D.L. Turner, A.V. Xavier, Cooperativity between electrons and protons in a monomeric cytochrome c_3: the importance of mechano-chemical coupling for energy transduction, ChemBioChem 2 (2001) 831–837.
[33] I.J. Correia, C.M. Paquete, R.O. Louro, T. Catarino, D.L. Turner, A.V. Xavier, Thermodynamic and kinetic characterization of trihaem cytochrome c_3 from *Desulfuromonas acetoxidans*, Eur. J. Biochem. 269 (2002) 5722–5730.
[34] P.M. Pereira, I. Pacheco, D.L. Turner, R.O. Louro, Structure–function relationship in type II cytochrome *c3* from *Desulfovibrio africanus*: a novel function in a familiar heme core, J. Biol. Inorg. Chem. 7 (2002) 815–822.
[35] M. Pessanha, R.O. Louro, I.J. Correia, E.L. Rothery, K.L. Pankhurst, G.A. Reid, S.K. Chapman, D.L. Turner, C.A. Salgueiro, Thermodynamic characterization of a tetrahaem cytochrome isolated from a facultative aerobic bacterium, *Shewanella frigidimarina*: a putative redox model for flavocytochrome c_3, Biochem. J. 370 (2003) 489–495.
[36] M. Pessanha, L. Morgado, R.O. Louro, Y.Y. Londer, P.R. Pokkuluri, M. Schiffer, C.A. Salgueiro, Thermodynamic characterization of triheme cytochrome PpcA from *Geobacter sulfurreducens*: evidence for a role played in e^-/H^+ energy transduction, Biochemistry 45 (2006) 13910–13917.
[37] J.S. Park, T. Ohmura, K. Kano, T. Sagara, K. Niki, Y. Kyogoku, H. Akutsu, Regulation of the redox order of four hemes by pH in cytochrome c_3 from *D. vulgaris* Miyazaki F, Biochim. Biophys. Acta 1293 (1996) 45–54.
[38] I.B. Coutinho, A.V. Xavier, Tetraheme cytochromes, Methods Enzymol. 243 (1994) 119–140.
[39] R.O. Louro, Proton thrusters: overview of the structural and functional features of soluble tetrahaem cytochromes c_3, J. Biol. Inorg. Chem. 12 (2007) 1–10.
[40] G. Simonneaux, A. Bondon, Mechanism of electron transfer in heme proteins and models: the NMR approach, Chem. Rev. 105 (2005) 2627–2646.
[41] I.J. Correia, C.M. Paquete, A. Coelho, C.C. Almeida, T. Catarino, R.O. Louro, C. Frazao, L.M. Saraiva, M.A. Carrondo, D.L. Turner, A.V. Xavier, Proton-assisted two-electron transfer in natural variants of tetraheme cytochromes from *Desulfomicrobium* Sp. J. Biol. Chem. 279 (2004) 52227–52237.
[42] R. Delgado, J.J.R.F. Da Silva, M.T.S. Amorim, M.F. Cabral, S. Chaves, J. Costa, Dissociation constants of Bronsted acids in D_2O and H_2O: studies on polyaza and polyoxa-polyaza macrocycles and a general correlation, Analytica Chimica Acta 245 (1991) 271–282.
[43] C. Bartels, T. Xia, M. Billeter, P. Güntert, K. Wüthrich, The program XEASY for computer-supported NMR spectral analysis of biological macromolecules, J. Biomol. NMR 6 (1995) 1–10.
[44] D.L. Turner, Obtaining ligand geometries from paramagnetic shifts in low-spin haem proteins, J. Biol. Inorg. Chem. 5 (2000) 328–332.
[45] M.A. Piçarra-Pereira, D.L. Turner, J. LeGall, A.V. Xavier, Structural studies on *Desulfovibrio gigas* cytochrome c_3 by two-dimensional ^{1}H-nuclear-magnetic-resonance spectroscopy, Biochem. J. 294 (1993) 909–915.
[46] M.P. Williamson, J. Kikuchi, T. Asakura, Application of ^{1}H NMR chemical shifts to measure the quality of protein structures, J. Mol. Biol. 247 (1995) 541–546.
[47] P.L. Dutton, Redox potentiometry: determination of midpoint potentials of oxidation–reduction components of biological electron-transfer systems, Methods Enzymol. 54 (1978) 411–435.
[48] T. Catarino, Thermodynamic and kinetic modelling of the redox properties of tetraheme cytochromes c_3, Ph.D Thesis, Instituto de Tecnologia Química e Biológica, Universidade Nova de Lisboa, Lisbon, 1998.
[49] M. Pessanha, E.L. Rothery, R.O. Louro, D.L. Turner, C.S. Miles, G.A. Reid, S.K. Chapman, A.V. Xavier, C.A. Salgueiro, Redox behaviour of the haem domain of flavocytochrome c_3 from *Shewanella frigidimarina* probed by NMR, FEBS Lett. 578 (2004) 185–190.
[50] J.M. Hudson, K. Heffron, V. Kotlyar, Y. Sher, E. Maklashina, G. Cecchini, F.A. Armstrong, Electron transfer and catalytic control by the iron–sulfur clusters in a respiratory enzyme, *E. coli* fumarate reductase, J. Am. Chem. Soc. 127 (2005) 6977–6989.
[51] V.B. Paixão, C.A. Salgueiro, L. Brennan, G.A. Reid, S.K. Chapman, D.L. Turner, Solution structure of a tetrahaem cytochrome from *Shewanella frigidimarina* reveals a novel family structural motif, Biochemistry 47 (2008) 11973–11980.
[52] E. Harada, J. Kumagai, K. Ozawa, S. Imabayashi, A.S. Tsapin, K.H. Nealson, T.E. Meyer, M.A. Cusanovich, H. Akutsu, A directional electron transfer regulator based on heme-chain architecture in the small tetraheme cytochrome *c* from *Shewanella oneidensis*, FEBS Lett. 532 (2002) 333–337.
[53] C.C. Page, C.C. Moser, X. Chen, P.L. Dutton, Natural engineering principles of electron tunnelling in biological oxidation–reduction, Nature 402 (1999) 47–52.